Engineering Journal issn: 0125-8281

Article

Seismic Strengthening of Partial Infilled RC Frame with Upper Opening Using Ferrocement and Expanded Metal Mesh

Rattawit Amornpunyapat[1], Phaiboon Panyakapo[1,*], Anat Ruangrassamee[2], and Pochara Kruavit[3]

1 Department of Civil Engineering and Town Development, School of Engineering, Sripatum University, Bangkok 10900, Thailand
2 Department of Civil Engineering, Faculty of Engineering, Chulalongkorn University, Bangkok 10330, Thailand
3 Department of Civil Engineering, King Mongkut's University of Technology North Bangkok 10800, Thailand
*E-mail: phaiboon.pa@spu.ac.th (Corresponding author)

Abstract. Severe damage often occurs in typical low-rise commercial buildings with reinforced concrete (RC) infilled frames featuring openings on the ground floor during earthquakes. Common failure modes include shear failure due to short-column behavior, as well as flexural and shear failures at the ends of columns and beams. To improve the shear and flexural strength of beam-column joints and enhance the lateral strength and ductility of infilled masonry walls, this study proposes a strengthening method for partial infilled RC frame with upper opening. An analytical model was also developed to predict the lateral strength and ductility of the frames. This research investigates the strengthening behavior of partial infilled RC frame with upper opening, reinforced using ferrocement and expanded metal mesh. The specimens were subjected to constant vertical loads and cyclic lateral loads. The experimental study involved two full-scale, single-story and single-bay frames: (1) a control specimen with an upper panel opening (UPF-C) and (2) a specimen with an upper panel opening strengthened using ferrocement and expanded metal mesh (UPF-S).The results demonstrate that the UPF-S specimen exhibited greater lateral resistance, stiffness, and ductility compared to the control specimen (UPF-C). The strengthening method effectively mitigated damage to the RC infill frame by shifting the failure behavior of beam-column joints from shear failure to ductile failure. Finally, the experimental results were analyzed and compared with nonlinear analytical models. The proposed model yielded predictions closely aligned with the experimental findings, confirming its reliability and consistency.

Keywords: Partial infilled RC frame, upper opening, ferrocement, expanded metal mesh, seismic strengthening.

ENGINEERING JOURNAL Volume 29 Issue 8
Received 19 March 2025
Accepted 20 August 2025
Published 31 August 2025
Online at https://engj.org/
DOI:10.4186/ej.2025.29.8.167

DOI:10.4186/ej.2025.29.8.167

1. Introduction

The 2014 earthquake in Mae Lao District, Chiang Rai Province, Thailand, with a magnitude of 6.3 M_L, caused extensive damage to typical low-rise buildings, particularly commercial buildings with partial infilled reinforced concrete (RC) frames featuring upper openings. The primary failure mode of these buildings was shear failure of the columns due to short column behavior. The ground floor, which typically serves as the front elevation of these buildings, consisted of partial masonry walls with upper openings. Due to the structural interaction between the columns and masonry walls, diagonal compression forces developed in the masonry walls adjacent to the bottom of the columns. This interaction led to shear cracks in the columns, ultimately causing combined flexural and shear failure in the columns and beam ends.

To improve the seismic resistance of these buildings, it is crucial to enhance the shear and flexural resistance of the columns and beams, as well as the lateral resistance and ductility of partial infilled RC frame with upper openings.

Previous studies have investigated the impact of brick walls with openings on reinforced concrete frames. Abu Sayed Mohammad Akid et al. [1] analyzed the effects of walls with openings (such as doors and windows) compared to frames without masonry walls using software-based simulations under cyclic lateral forces. Their results indicated that brick walls with openings reduced the moment and shear resistance of the frame structure, primarily due to interaction forces between the frame and the masonry. Other studies [2]-[5] reported similar findings.

Research has consistently shown that brick walls with openings significantly impact the seismic performance of reinforced concrete frame structures. Consequently, the strengthened structures particularly plastered brick masonry walls vulnerable to earthquake damage has been a key focus for many researchers. Various strengthening techniques have been explored to enhance the earthquake resistance of masonry structures.

In previous studies, the effect of infill masonry walls on the performance of reinforced concrete frames was examined. Leeanansaksiri et al. [6] studied the behavior of masonry walls reinforced with ferrocement and expanded metal mesh. Their results showed that the reinforced masonry walls exhibited higher strength, ductility, and energy dissipation than unreinforced walls. However, the strengthened wall caused stress concentrations at the upper corners of the masonry, leading to column failure. S. Longthong et al. [7] later developed reinforcement techniques for masonry walls, columns, and beams, improving resistance to shear damage and preventing corner failure due to compressive forces by using ferrocement with expanded metal mesh. Further research by S. Vincent Sam Jebadurai et al. [8] demonstrated that reinforcing brick walls with chicken mesh improved ductility, energy dissipation, lateral loadbearing capacity and lateral displacement capacity. Similarly, Thainswemong Choudhury et al. [9] found that small steel reinforcement strips significantly enhanced the lateral resistance and ductility of masonry walls compared to unreinforced walls.

While previous studies primarily focused on the reinforcement of infill masonry walls, the effects of masonry walls with openings despite their significant impact on structural performance were not thoroughly investigated. To address this gap, Sarwat Hassan Ahmed et al. [10] compared the reinforcement of brick walls with openings using external steel reinforcement and ferrocement. Their tests showed that externally reinforced walls provided high lateral resistance and durability, though they exhibited lower ductility than ferrocement reinforced walls. Xianhua Yao et al. [11]-[13] also investigated reinforcement techniques using ferrocement with welded steel mesh and basalt fiber cloth in masonry walls with openings. Both methods effectively improved lateral resistance and ductility. Further advancements in ferrocement reinforcement included the use of welded mesh and expanded metal mesh, which provided superior lateral resistance, ductility, and energy dissipation. Later, Ismail et al. [16-17] studied ferrocement reinforcement of masonry walls with openings in single-story houses. The strengthened masonry significantly improved shear strength and prevented cracking under lateral forces compared to unreinforced walls. Salvador Ivorra et al. [18] demonstrated that cement reinforced with fiber cloth improved shear resistance and energy dissipation, reduced crack and enhanced lateral resistance. In the same year, Tong Li et al. [19] studied masonry walls with openings reinforced with engineered cementitious composites (ECC). Their findings showed that ECC improved strength, durability, and energy dissipation while effectively reducing crack propagation. Fauzan et al. [20] further investigated the reinforcement of damaged masonry walls using ferrocement with a bandage system and it was demonstrated that the increased reinforcement and layering effectively prevented severe damage. Subsequent research by S. Panyamul et al. [21] focused on using expanded metal mesh for reinforcement to improve shear resistance in short columns. Their tests revealed that both types of mesh provided enhanced shear resistance, ductility, and energy dissipation. Additionally, it was observed that the expanded metal mesh with a higher specific surface area was more effective in reducing surface cracking of the concrete and preventing further propagation. Furthermore, other researchers studied ferrocement reinforcement for shear enhancement in columns. It was found that the increase of the number of wire mesh layers significantly improved the shear strength, ductility, and overall strength of the columns [22], [23]. The following year, Phawe Suit Theint et al. [24] developed an external high-strength steel rod collars reinforcement method for columns to improve shear strength. It was found that closer stirrup spacing enhanced shear strength, ductility, and bending resistance.

While most of the previous research focused on the reinforcement of masonry walls alone, limited attention has been given to reinforcing the entire structural system

including columns and beams under combined bending and shear forces. This study aims to develop a new reinforcement technique for the entire structure, incorporating columns and beams with partial brick masonry walls, to enhance earthquake resistance. Specifically, this study focuses on ferrocement reinforcement with expanded metal mesh, a method recognized in ACI 549 [25] for its ease of installation, cost-effectiveness, and local availability. Two specimens were tested: a) partially infilled frame featuring an upper opening, b) strengthened partial brick masonry walls with upper opening, in which masonry walls were strengthened on both sides to enhance lateral resistance and ductility. Additionally, external steel reinforcement was added to the columns to enhance the bending moment capacity. Finally, the laboratory test results were compared with the proposed analytical model.

2. Model of Strengthened Specimen

2.1 Strengthened RC Bare Frame

The strengthened model of the rigid reinforced concrete (RC) frame is shown in Fig. 1a. The strengthened method employs the ferrocement technique, utilizing expanded metal mesh confinement along the full height of the column. The intention is to resist lateral forces from the masonry wall, which could cause shear failure in the short columns on both sides of the window openings. Meanwhile, the strengthened technique of beam is achieved by applying ferrocement reinforcement at the beam ends over a length approximately 2.5 times the beam depth. This reinforcement is necessary because lateral forces induce moments that transfer from the column-beam connection to the beam ends. Therefore, ferrocement reinforcement is applied over a length equivalent to the plastic hinge length, which may develop at the beam ends.

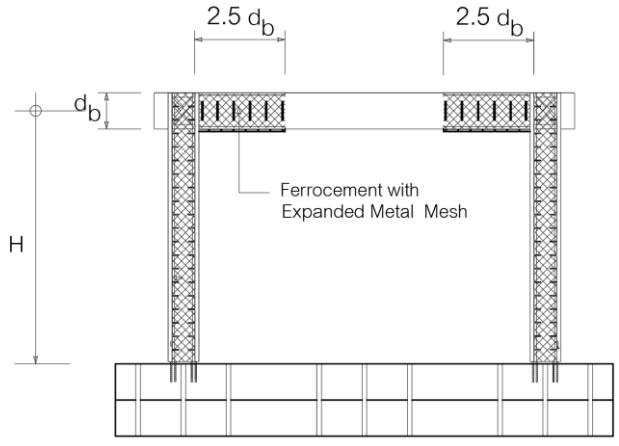

(a) Model of RC Bare Frame

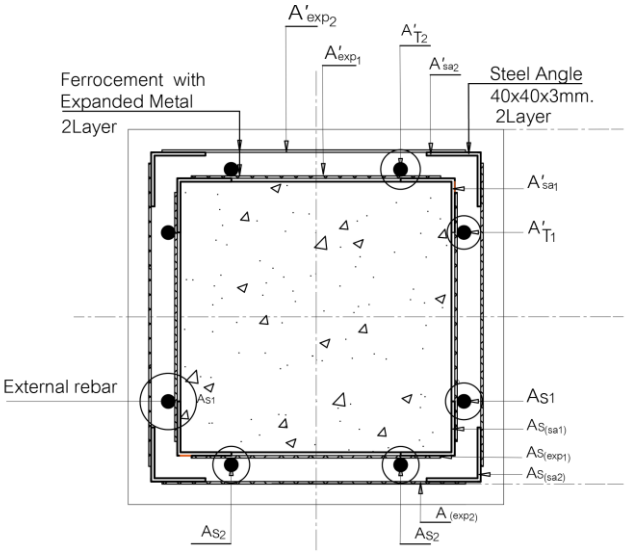

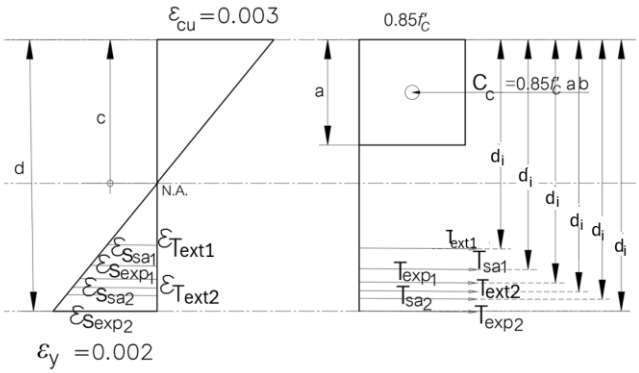

(b) Stress block of RC column

Fig. 1. Strengthened of RC Bare Frame.

From Fig. 1b, which illustrates the strain and stress distribution of the reinforced concrete column, the maximum moment resistance capacity of the strengthened RC column can be determined by calculating the moments about the centroid of the compressive force C_c. This includes the moment resistance of the existing column with external longitudinal reinforcement and the moment resistance of the ferrocement-confined RC column under bending, as shown in Eq. (1) as follows:

$$M_{sc} = (M_n^F + M_{ext}) + M_o \quad (1)$$

where M_{sc} is the moment resistance capacity of the strengthened RC column; M_n^F is the moment resistance capacity of the ferrocement confinement of the original RC column; M_{ext} is the moment resistance capacity of the external bar reinforcement; M_o is the moment resistance capacity of the original RC column.

The calculation involves taking the tensile moment about the centroid of the concrete compressive stress block, following the recommendations of ACI 549 [25].

This standard assumes that the primary moment is generated solely by tensile forces, while compressive forces are neglected due to their minimal effect.

The moment resistance of the ferrocement and the external longitudinal reinforcement can be calculated as follows:

$$M_n^F + M_{ext} = \sum_{i=1}^{2} T_{\exp i}\left(d_i - \frac{a}{2}\right) + \sum_{i=1}^{2} T_{sai}\left(d_i - \frac{a}{2}\right) + \sum_{i=1}^{2} T_{exti}\left(d_i - \frac{a}{2}\right) \quad (2)$$

where T_{expi}, T_{sai}, T_{exti} are the tensile forces of expanded metal mesh, steel angle, and the external bar, respectively; and d_i represents the lever arm of each corresponding force.

The moment resistance of the existing column is calculated as proposed by Tumialan et al. [26], as shown in Eq. (3).

$$M_o = A_{st} f_y g d + 0.5 N d\left(1 - \frac{N}{b d f_c^{'}}\right) \quad (3)$$

where A_{st} is the cross-sectional area of the reinforcement resisting tensile forces of the original RC column; f_y is the tensile strength of the reinforcement at yield point; $f_c^{'}$ is the compressive strength of the concrete; g is the ratio of the spacing between the tensile and compressive reinforcement, which is proportional to the depth of the original column; b, d are the width and depth of the original RC column; N is the axial compressive force in the column.

The lateral resistance capacity of the strengthened rigid bare frame can be calculated from Eq. (4).

$$R_{BFS} = \frac{2\left(M_{sc} + M_{Pj}\right)}{H} \quad (4)$$

The lateral resistance of the existing bare frame (R_{BF}) can be calculated using Eq. (5).

$$R_{BF} = \frac{2\left(M_o + M_{pj}\right)}{H} \quad (5)$$

where M_{Pj} is the minimum moment resistance between M_{pc}, M_{pb}, M_j.

M_{pc} is the plastic moment resistance in the column.

M_{pb} is the plastic moment resistance in the beam.

M_j is the moment resistance of the column-beam joint.

2.2 Model of Strengthened Partial Infilled Frames with Upper Opening

The modeling of strengthened partial infilled frames with an upper opening is shown in Fig. 2. A reinforced concrete rigid frame with a full-width window opening is used as the prototype structure. The strengthening of columns and beams follows the ferrocement technique described earlier. The masonry wall consists of a lower infill panel with a height of h_1, while the upper portion features a wide window opening with a height of h_o. The lower infill panel is strengthened using ferrocement techniques with expanded metal mesh. To analyze the internal forces within the infill panel, the Equivalent Strut Model (ESM) is used to simulate its load-bearing behavior. Given that the typical failure mode of the infill panel is diagonal cracking, the maximum lateral force P is determined by summing the resistance force of the strengthened bare frame (R_{BFS}) and the horizontal resistance force of the lower infill panel (F_1). Thus, P is calculated using the following equation:

$$P = R_{BFS} + F_1 \cos\theta_1 \quad (6)$$

where F_1 is the diagonal compression strut forces for the lower partial infill panel, it can be calculated as follows.

$$F_1 = w_1 t f_a \quad (7)$$

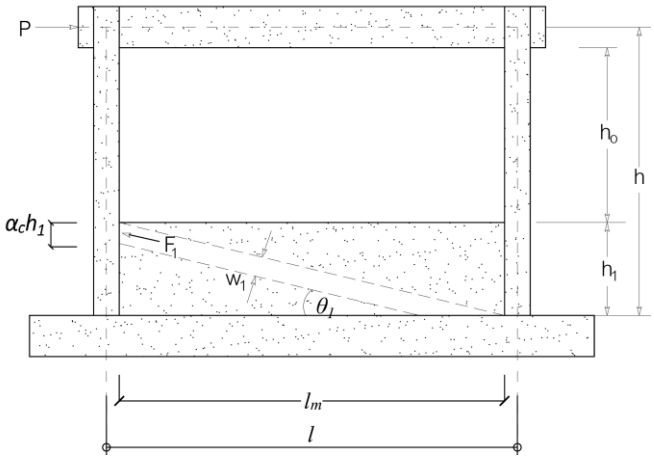

Fig. 2. Partial infilled RC frame with upper opening.

where f_a is the allowable compressive stress of strengthened masonry prism, can be calculated as $f_a = 0.6\phi f_m^{'}$, $\phi = 0.65$.

$f_m^{'}$ is the compressive strength of strengthened masonry prism.

t is the thickness of strengthened masonry infill panel.

θ_1 is the angle of the diagonal strut relative to the horizontal for the lower infill panel.

The equivalent strut of the lower infill panels has width w_1. It was assumed that the permissible compressive stress acting on the contact surface between the infill and the column have width $\alpha_c h_1$, as proposed by Saneinejad and Hobbs [27]. Therefore, the width of the equivalent strut can be calculated as follows.

$$w_1 = \alpha_c h_1 \frac{l_m}{\sqrt{h_1^2 + l_m^2}} = \alpha_c h_1 \cos\theta_1 \quad (8)$$

where

$$\alpha_c = \frac{1}{h}\sqrt{\frac{2M_{pj} + 2\beta_c M_{pc}}{\sigma_c t}} \quad (9)$$

$$\sigma_c = \frac{f_m'}{\sqrt{1 + 3\mu^2 r^4}} \quad (10)$$

μ is the coefficient of friction of the frame and infill interface.

r is the aspect ratio of the frame ($r = h/l$).

β_c is the reduction factor for columns which uses a value equal to 0.2.

The procedure to calculate the lateral resistance of the strengthened RC frame and the strengthened partial infilled frame are summarized in the flowchart, as shown in Fig. 3.

(1) Define Geometric and Material Properties:
-Specify the cross-sectional dimensions, material strengths, and reinforcement details for beams, columns, and masonry infill panels.

↓

(2) Calculate Moment Resistance of Columns:
-For strengthened columns (M_{sc}), compute total moment resistance using Eq. (1).
-The contributions from ferrocement layers (M_n^F), external reinforcements (M_{ext}), and the original column are determined using Eqs. (2) and (3), respectively.

↓

(3) Evaluate Lateral Resistance of Bare Frame:
-Use the strengthened moment capacity to compute the lateral resistance of the strengthened frame (R_{BFS}) (Eq. 4).
-Similarly, use the original column capacity to determine the lateral resistance of the bare frame (R_{BF}) (Eq. 5).

↓

(4) Determine the Lateral Resistance of the strengthened Partial Infilled Frame:
-Combine the lateral resistance of the strengthened bare frame and the horizontal resistance of the lower infill panel to obtain the total lateral capacity (P), Eq. (6).

↓

(5) Determine Diagonal Compressive Force in Infill Panel:
-The diagonal compressive strut force(F_1) in the masonry panel is computed from Eq. (7).
-The strut width and the corresponding parameters w_1, σ_c, α_c are computed from Eq. (8), (9), and (10), respectively.

Fig. 3. Method for Calculating the Resistance of Partial Infilled Frame Models.

3.1. Properties of Specimens

The prototype specimens of reinforced concrete frames were prepared for laboratory testing. The concrete mix was designed to achieve a cylindrical compressive strength of 21 MPa at 28 days.

For brick masonry, the brick has a dimension of 50 mm in width, 160 mm in length, and 60 mm in height, as shown in Fig. 4. The mortar used for bedding is a mix of cement and sand in a 1:4 ratio, with an ultimate strength of 7.22 MPa at 28 days. Additionally, the plaster mortar for ferrocement was designed with a cement-to-sand ratio of 1:2 by weight and a water to cement ratio of 0.45. The yield strength of the plaster mortar at 28 days is 22.25 MPa, in accordance with ASTM C349-97 [28].

For the columns and beams, longitudinal reinforcement with a diameter of 16 mm and a yield strength of 400 MPa was used, in accordance with the TIS 24-2559 standard [29]. Transverse reinforcement with a diameter of 6 mm was used for the columns and beams, following the TIS 20-2543 standard [30], with a tensile strength of 240 MPa. Additionally, external reinforcement for the columns was designed with a diameter of 12 mm and a tensile strength of 400 MPa, as per the TIS 24-2559 standard [29], to enhance the lateral bending resistance of the columns. The mechanical properties of the reinforcement steel are presented in Table 1.

For this test, expanded metal sheets were used as reinforcement for ferrocement. These sheets consist of perforated steel arranged in a diamond pattern, as detailed in Fig. 5. The basic properties of the expanded metal sheets are presented in Table 2, in accordance with the JIS G3351-1987 standard [31]. The expanded metal sheets have a yield strength of 337 MPa and an ultimate tensile strength of 400 MPa.

DOI:10.4186/ej.2025.29.8.167

Table 1. Mechanical properties of steel bars.

Type Rebar	D (mm)	f_y (MPa)	f_u (MPa)	E (MPa)
DB16 (SD40)	16	400	560	$2.06x10^5$
DB12 (SD40)	12	400	560	$2.06x10^5$
RB9 (SR24)	9	240	390	$2.06x10^5$
RB6 (SR24)	6	240	390	$2.06x10^5$

Table 2. Physical properties of expanded metal mesh.

Type No.	A (mm)	B (mm)	C (mm)	D (mm)	Weight (Kg./m^2)
1	20	8.6	0.6	-	0.69
2	30.5	12	2.3	3.0	6.42

Fig.4. Brick size 50x160x60 mm.

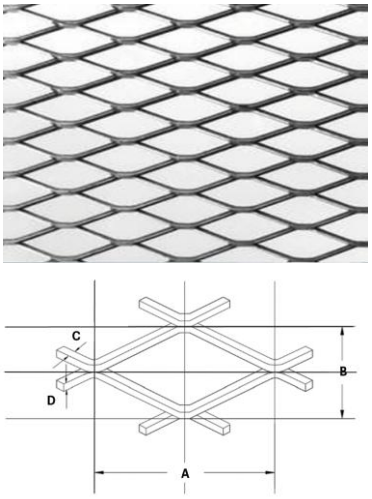

Fig. 5. Details of expanded metal mesh.

3.2. Test Specimens

In this section, the reinforced concrete bare frame with partial infill and an upper opening was selected as the model specimen. The reinforced concrete rigid frame has dimensions of 4,000 mm in width and 3,000 mm in height. The square columns have a dimension of 250 mm in width, while the beam is 200 mm in width and 400 mm in height. Additionally, the base concrete has a dimension of 1,500 mm in width, 5,500 mm in length, and 400 mm in height. Details of the bare frame are shown in Fig. 6a.

For the partially infilled frame, bricks were laid in a half-scale unit horizontally to a height of 750 mm from the base, aligning with the bottom of the window along the length of the wall. The cement mortar mix followed a cement-to-sand ratio of 1:4, in accordance with general construction standards. A lintel was installed at the top of the wall panel at a height of 900 mm to prevent lateral out-of-plane instability. Both sides of the brick wall were plastered with mortar (cement-to-sand ratio of 1:2) to achieve a smooth surface, with a thickness of approximately 10 mm. The control specimen (UPF-C) is shown in Fig. 6b, while the strengthened partial-infilled RC frame with upper openings, reinforced with ferrocement and expanded metal (UPF-S), is shown in Fig. 6c.

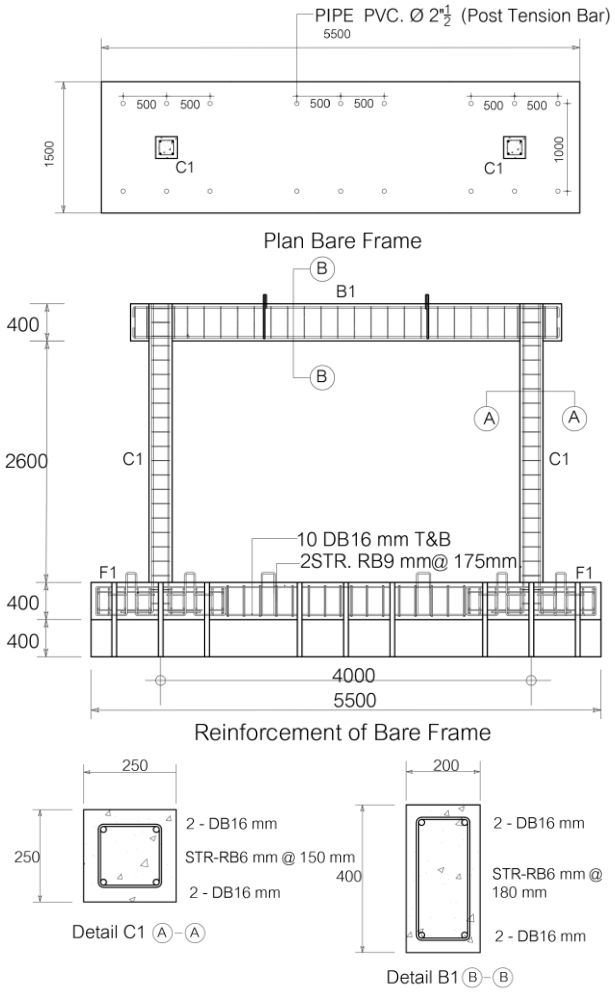

(a) Detail of RC Bare Frame

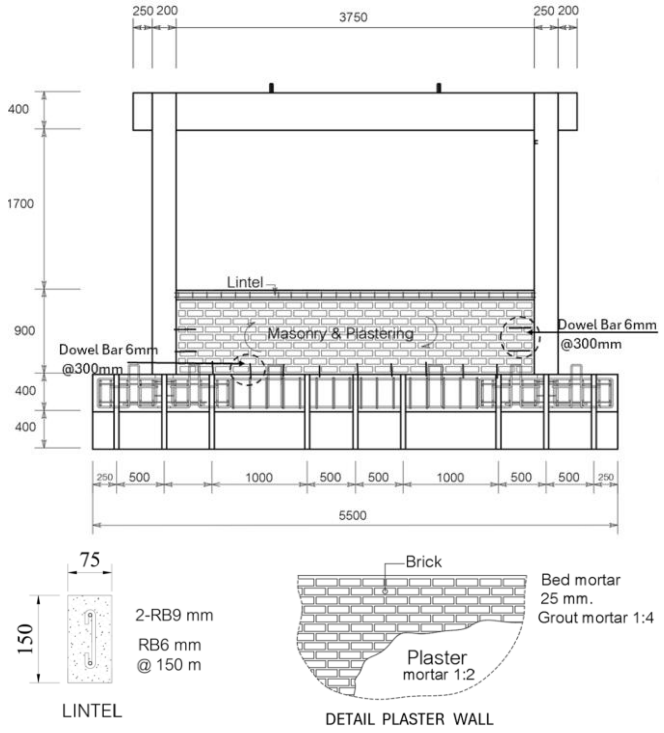

(b) Details of UPF-C

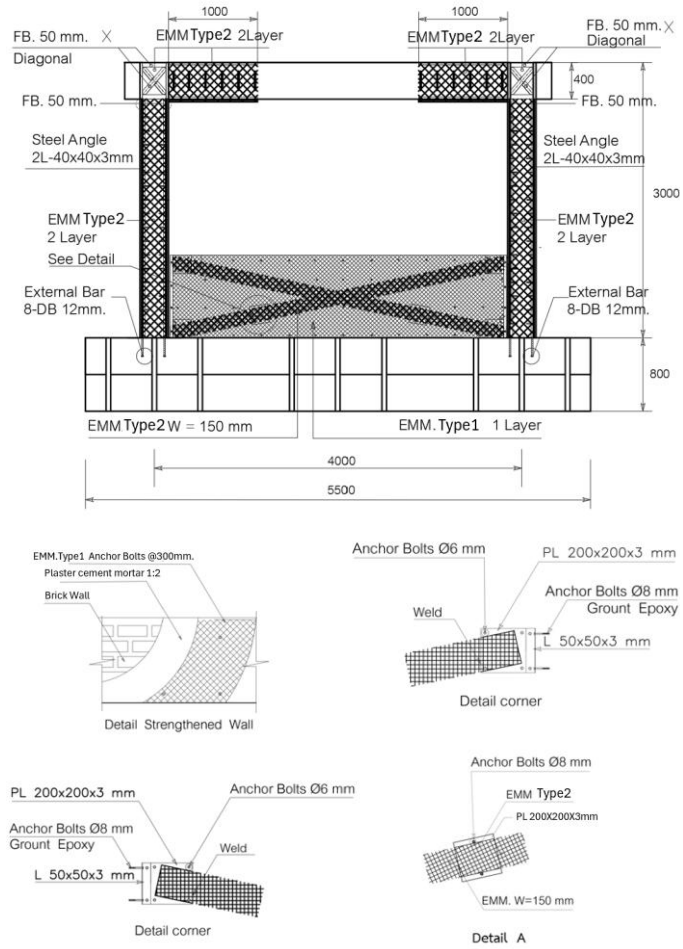

(c)Detail Strengthened of UPF-S

Fig. 6. Model of partial infilled RC Bare Frame.

3.3. Strengthening Method for the Partial Infilled Frame

To strengthen the partially infilled RC frame with an upper opening, the strengthening process of UPF-S was divided into two steps:

(1) Strengthening of the RC Frame, as shown in Fig. 7a. The surface of the existing concrete columns was roughened to improve adhesion. Next, 40×40×3 mm steel angles were installed at all four corners of the columns to reduce stress concentrations and the sharpness of the expanded metal mesh. Additionally, 50×50×3 mm steel angles were installed at the lower corners of the beam ends, with a length approximately 2.5 times the depth of the beam. The first layer of expanded metal mesh (type 2) was then installed and secured using the steel angles, as shown in Fig. 7b. Subsequently, the RC columns were externally reinforced by embedding 12 mm rebars into the concrete base and beneath the beam, with depths of approximately 200 mm and 100 mm, respectively, as shown in Figs. 7c and 7d. These rebars were bonded with epoxy adhesive to increase the bending strength of the columns. A cement mortar layer was then applied over the expanded metal mesh, maintaining a thickness of 25 mm, with a cement-to-sand ratio of 1:2. The second layer of steel angles and expanded metal mesh (type 2) was installed in the same manner as the first step. The expanded metal mesh was secured using L-shaped steel rods, 9 mm in diameter, 100 mm deep, and spaced 150 mm apart along the entire column height. These rods were bonded with epoxy adhesive, as shown in Fig. 7e. Finally, a cement mortar layer was applied over the expanded metal mesh, maintaining a thickness of approximately 25 mm.

(2) Strengthening of the Partial Infill Panel. Firstly, the surface of the brick wall panel was prepared to achieve a smooth finish. Then, the expanded metal mesh (type 1) was attached flat on both sides to enhance wall ductility, secured with 8 mm diameter bolts, spaced approximately 300 mm apart in a grid pattern. Additionally, 50×50×3 mm steel angles were installed at the four corners of the wall over the expanded metal mesh to enhance joint strength between the wall and columns. Next, a second layer of expanded metal mesh (type 2), 150 mm wide, was installed diagonally in an "X" pattern on both sides of the wall to resist the diagonal tensile force of the brick masonry wall, as shown in Fig. 7f. Finally, a layer of cement mortar was applied over the expanded metal mesh, with a thickness of approximately 12.5 mm. The plaster mortar had a cement to sand ratio of 1:2 for ferrocement.

DOI:10.4186/ej.2025.29.8.167

(a) Strengthened of UPF-S

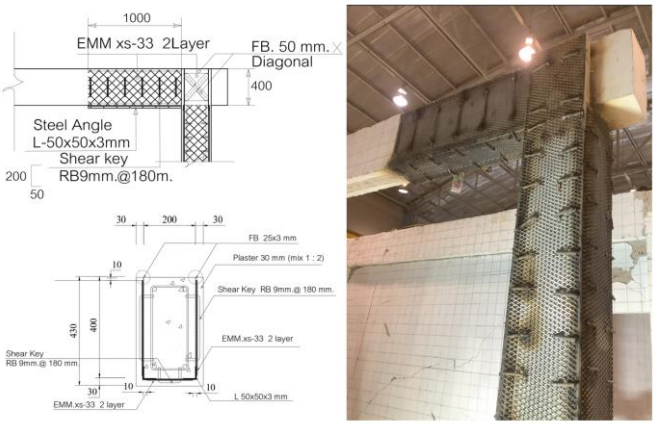

(b) Detail of strengthened beam

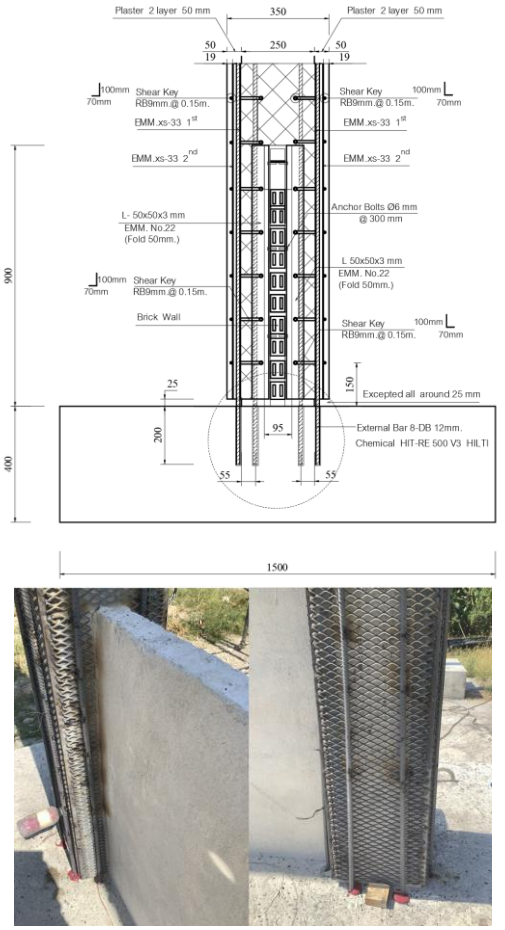

(c) Detail of external bars embedded into the concrete base

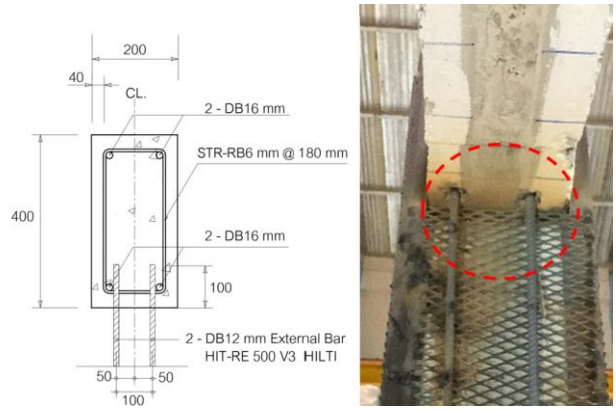

(d) Section Steel bars embedded in the beam

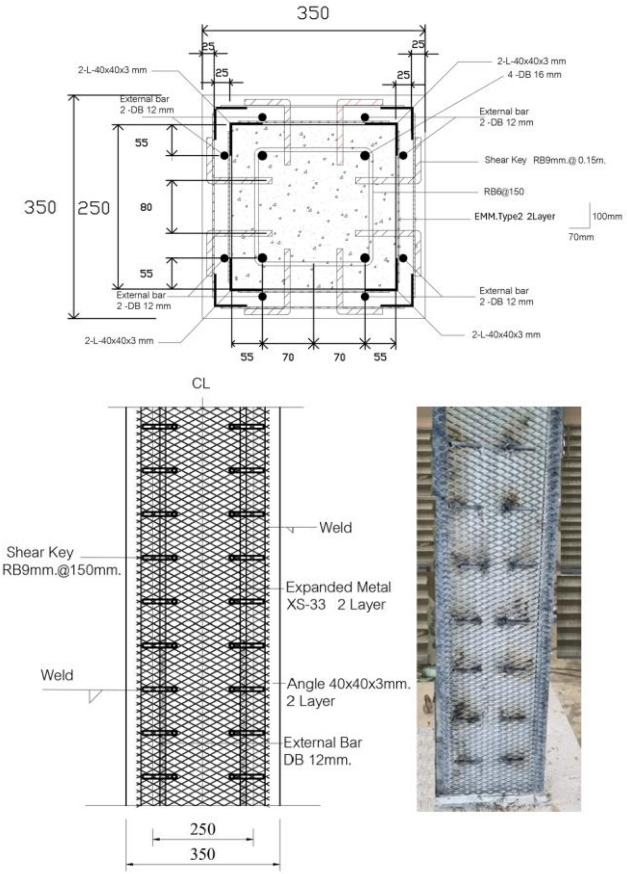

(e) Detail of strengthened column

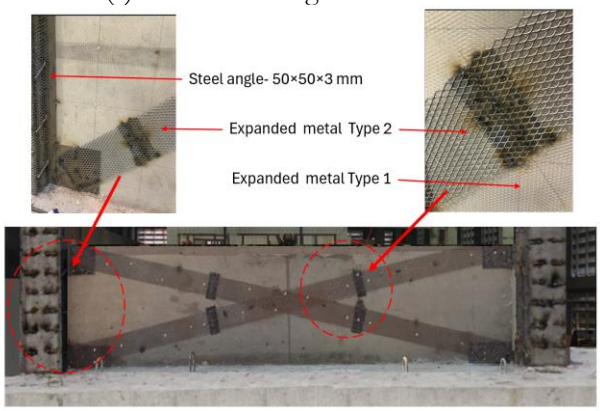

(f) Detail of strengthened wall and joints flanking the column

Fig. 7. Details of strengthened masonry wall and Bare Frame.

3.4. Experimental Programs

The procedure for testing the partially infilled frame specimens in the laboratory is illustrated in Fig. 8a. First, the foundation was anchored to the strong floor using 32 mm diameter bolts to prevent frame displacement. Then, hydraulic jacks were installed at the top of both concrete columns to apply a constant vertical compressive load of 300 kN. For lateral loading, an MTS hydraulic actuator with a capacity of 1,500 kN was used. The actuator was installed at the center of the beam at a height of 3.60 meters above the strong floor and securely fixed to the strong wall. While the hydraulic actuator pushed the frame forward, the frame was pulled back in the opposite direction by a pair of high-strength steel rods with a diameter of 32 mm. Horizontal displacement of the specimen was recorded using displacement sensors at the beam center. Additional instruments measured moment curvature, column curvature, and displacement of the strong wall. All data were recorded by a data logger for further processing. The specimen was tested under cyclic loading, following the lateral displacement control protocol in FEMA 461 [32], as shown in Fig. 8b. Testing started with a displacement of 0.10% up to 0.50%, increasing incrementally by 0.25% until failure, at which point the test was terminated. The test continued until the strength was reduced to approximately 80% of its maximum strength; the test was then terminated.

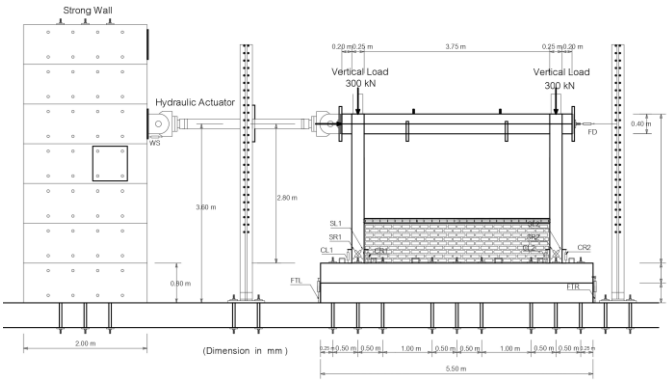

(a) Test setup

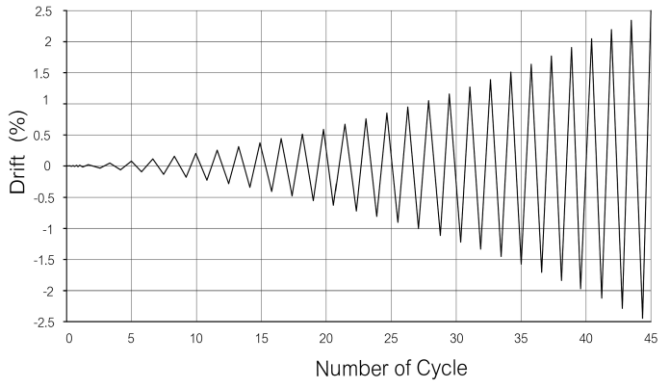

(b) Lateral loading

Fig. 8. Test setup and lateral loading.

4. Discussion of Experimental Results

4.1. Failure Mode of Infilled Wall Frame with Upper Opening

For the control specimen (UPF-C), the lateral load began to push the specimen to a displacement corresponding to a 0.50% drift. (Fig. 9a), leading to the formation of cracks at the joint between the column and the upper wall, along with minor cracks in the column. Additionally, the lower wall began to separate slightly from the base floor. As the lateral load increased to a displacement range of 0.5%–1.0%, the cracks at the wall-column joint started to widen, and minor cracks appeared at the beam-column joint due to flexural failure. With a further increase in lateral load to a displacement of 1.0%–1.5% (Fig. 9b), the cracks at both the beam-column and wall-column joints were widened noticeably. As the displacement increased to 1.5%–2.5% (Fig. 9c), the column-beam joints on both sides of the building frame experienced severe concrete cracking due to flexural failure at the upper ends of the columns, exhibiting a weak-column strong-beam failure mode. Additionally, both columns experienced diagonal cracks at an angle of approximately 60 degrees at a height of 90 cm, indicating shear failure (Fig. 9d). This was attributed to the compression force along the diagonal of the masonry wall, resulting from the interaction behavior between the column and the wall. Finally, when the displacement reached the maximum target of 3.0%, the lateral resistance of the structure decreased to approximately 80% of its maximum strength, leading to the termination of the test, as shown in Fig. 9e.

(a) Story drift at 0.5%

(b) Story drift at 1.5%

DOI:10.4186/ej.2025.29.8.167

(c) The flexural and shear cracks of column-beam joint

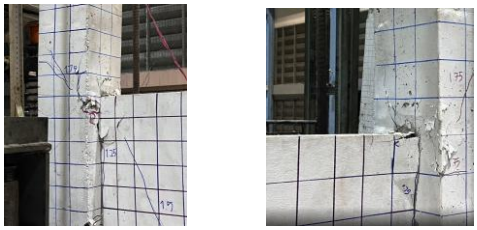

(d) The shear, flexure, diagonal compression of the column-flanking wall joints

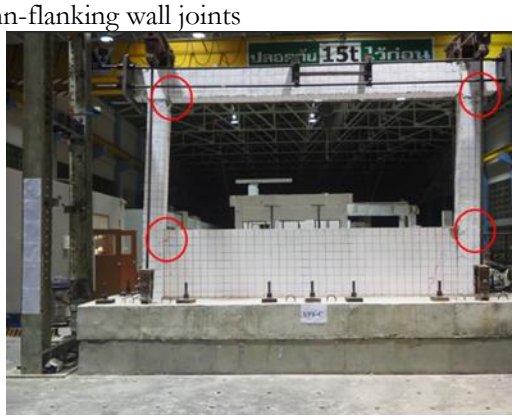

(e) Story drift at 3.0%

Fig. 9. Failure of the UPF-C.

For the strengthened specimen (UPF-S), when the lateral load was applied up to 0.50% drift (Fig. 10a), minor hairline cracks appeared in the masonry wall. As the displacement increased to 1.00%–1.50% (Fig. 10b), the cracks occurred between the brick wall and column interface due to the interaction between the wall and the column. Additionally, minor surface plaster cracks were observed at the beam-column joint.

When the displacement reached 1.50%-2.5% drift (Fig. 10c), the wall-column joint exhibited wider cracks, with plaster peeling off at the top and bottom corners due to compressive forces on the wall. Vertical cracks formed at the beam-column joint, accompanied by plaster peeling at the left and right corners of the column (Fig. 10d). Additionally, damage at the base of the right column caused concrete debris to detach. This damage occurred as the external reinforcement at the lower end approached the yield point, as shown in Fig. 10e.

As the lateral force increased up to 3.0% drift (Fig. 10e), the cracks at the wall-column joint did not extend further, and the cracks at the beam-column joint remained stable. No significant damage was observed in the masonry wall, aside from minor cracks. However, the frame's resistance capacity decreased rapidly due to the failure of the reinforcement at the base of the column, approximately 100 mm from the foundation. This failure occurred when the strain of external reinforcement exceeded the yield point at 0.002, as depicted in Fig. 10f.

Finally, at 4.0% displacement, the lateral force resistance capacity of the specimen dropped to approximately 60% of its maximum strength, leading to the termination of the test. It was observed that the column failed at the column-beam joint because the joint was weaker than both the column and the beam. Additionally, the wall panel experienced diagonal cracks due to the compression strut force acting along the diagonal direction. Furthermore, the cracks caused separation between the infilled wall and frame. However, the overall structural integrity remained intact. The use of expanded metal mesh for strengthening effectively reduced severe failures caused by shear and bending of the columns while enhancing the ductility of the wall. Additionally, the external bar reinforcement carried tensile forces up to the yield point, demonstrating its effectiveness, as shown in Fig. 10g.

(a) Story drift at 0.50%

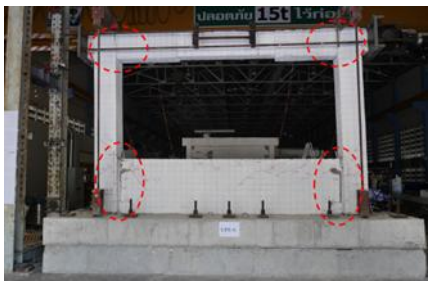

(b) Story drift at 1.50%

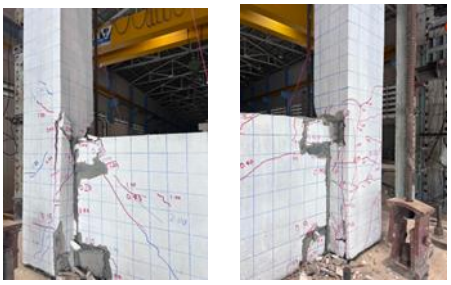

(Left) (Right)

(c) Diagonal compression cracks of column-flanking wall joints

(Left) (Right)

(d) Vertical cracks of beam-column joints

(Left) (Right)

(e)The external bars reinforcement failed, deformed, and bent at the column base

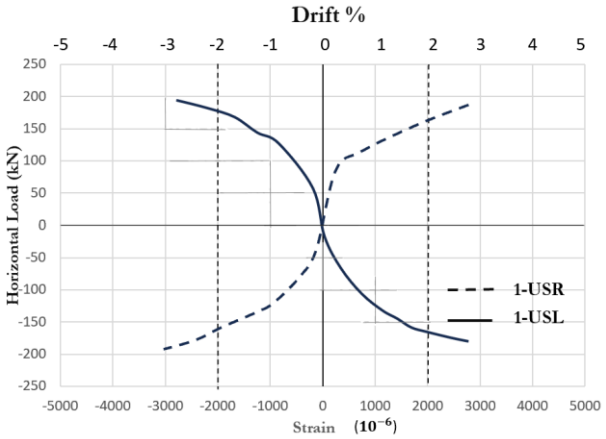

(f) The relationship between stress and strain of the external bars at the yield point 0.002 of columns

(g) Story drift at 4.00%

Fig. 10. Failure of the strengthened UPF-S.

4.2. Hysteresis Behavior

The relationship between force and lateral displacement of the partial infilled RC frames with upper opening of UPF-C and UPF-S are shown in Fig.s 11(a) and 11(b). The enveloped curve between the upper opening RC frames of the UPF-C and UPF-S are shown in Fig. 11(c).

For the partial infill RC frame (UPF-C), the frame exhibits elastic behavior up to a drift value of 0.25%, corresponding to a lateral displacement of approximately 11.33 mm. Beyond this point, the frame starts into inelastic behavior as the displacement increases, reaching a maximum load of approximately 97.80 kN at a lateral displacement of 45.13 mm (1.5% drift). Subsequently, the frame's resistance gradually decreases until the drift reaches 3%, at which point the test was terminated.

For the strengthened partial infill RC frame (UPF-S), the frame initially exhibits linear behavior up to a drift value of approximately 0.30%, with a lateral displacement of 7.89 mm. Beyond this point, nonlinear behavior was observed, reaching a maximum lateral displacement of 67.60 mm at 2.25% drift and a peak load of 198.45 kN. After this stage, the frame can no longer maintain its structural integrity, leading to test termination at 4% drift. The hysteresis loop of the strengthened frame demonstrates greater energy dissipation and higher ductility compared to the original frame, indicating improved structural performance.

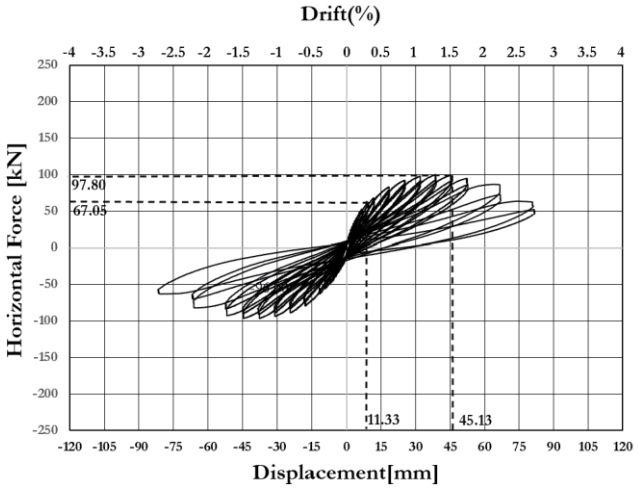

(a) UPF-C

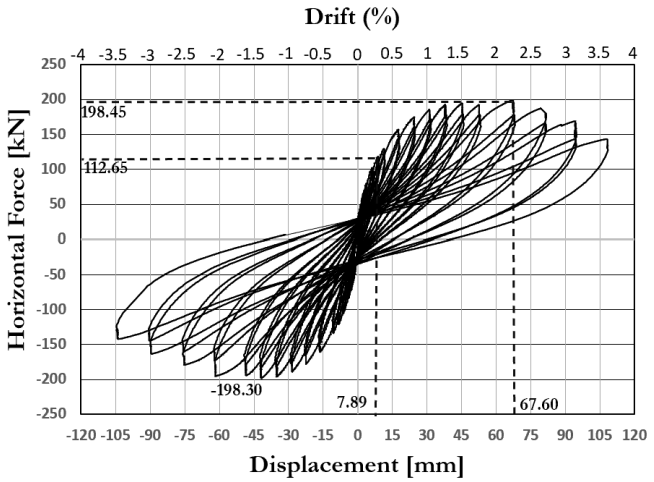

(c) UPF-S

DOI:10.4186/ej.2025.29.8.167

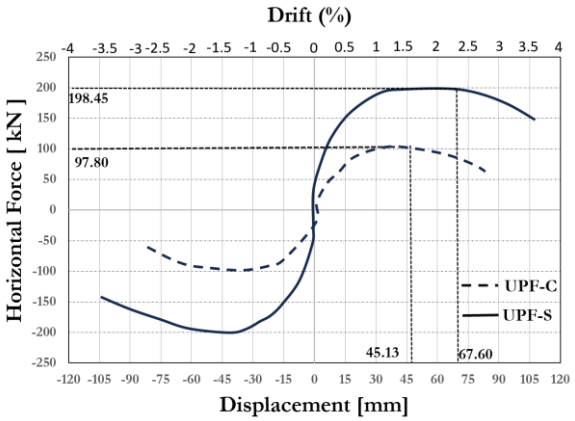

(d) Enveloped curves of UPF-C and UPF-S

Fig. 11. Hysteretic behaviors of the specimens.

4.3. Lateral Strength

The lateral strength of the masonry frame at the yield point can be determined as the intersection point of a bilinear curve of the initial strength and post-yield strength, suggested by ASCE 41-06 [33]. The test results, summarized in Table 4, indicate that the lateral resistance, stiffness, and ductility of the UPF-S specimen were 1.68, 2.41, and 1.94 times higher than those of the control specimen, respectively.

Meanwhile, the maximum strength results are presented in Table 5. The data reveal that the UPF-S specimen exhibited 2.04 times the maximum strength and 1.12 times the maximum displacement compared to the control UPF-C specimen. These improvements suggest that ferrocement reinforcement combined with external longitudinal rebar significantly enhances the lateral resistance of the frame while also increasing the ductility of the masonry wall.

Table 4. Stiffness and Ductility of UPF-C and UPF-S.

Structure	UPF-C	UPF-S
$V_y\,(kN)$	67.05	112.65
$\Delta_y\,(mm)$	11.33	7.89
$\Delta_u\,(mm)$	80.35	108.08
$k_0\,(kN/m)$	5.92	14.28
Ductility	7.09	13.75

Table 5. Maximum Strength of UPF-C and UPF-S.

Structure	UPF-C	UPF-S
$V_{\mathrm{m}}\,(kN)$	97.80	198.45
$\Delta_m\,(mm)$	45.13	67.60
$Drift_m\,(\%)$	1.50	2.50
$k_{\mathrm{sec}}\,(kN)$	2.17	2.94
$\Delta_u\,(mm)$	80.35	108.08
$Drift_u\,(\%)$	3.00	3.50

The parameters obtained from the design capacity of the UPF-C and UPF-S specimens include the moment capacity of the frame structure and the equivalent diagonal strut of the brick masonry wall, as summarized in Tables 6 and 7, respectively. These parameters were used to simulate the behavior of the wall-frame system with an upper opening. For both the bare frame and the strengthened frame, the lateral resistance capacity was calculated as 70 kN and 157.56 kN, respectively, based on Equations (1)– (5), as described earlier. Regarding the equivalent diagonal strut of the existing brick masonry wall, its resistance force (22.26 kN) and design strength of the partial infilled frame (92.26 kN) were determined. Similarly, for the ferrocement-strengthened brick masonry wall with expanded metal mesh, the equivalent diagonal strut resistance was 31 kN, and the strength capacity of the strengthened partial infilled frame was 188.56 kN. These values were obtained from calculations following Equations (6)– (10), as outlined earlier in this study.

Table 6. Moment capacity and Design capacity of the RC frame.

Structure	Existing Bare Frame	Strengthened Bare Frame
$M_{exc}\,(kN-m)$	57.69	57.69
$M_{pj}\,(kN-m)$	46.06	46.06
$M_n^F\,(kN-m)$	-	38.50
$M_{ext}\,(kN-m)$	-	78.40
$M_{sc}\,(kN-m)$	-	174.59
Lateral Resistance(kN)	70.00	157.56

Table 7. Design capacity of the masonry wall UPF-C and UPF-S.

Structure	Lateral Resistance of Bare Fram(kN)	Masonry wall(F) $F_1\cos\theta_1$ (kN)	Design Capacity (kN)
UPF-C	70.00	22.26	92.26
UPF-S	157.56	31.00	188.56

4.4. Analytical Modelling of specimens

The structural model with an upper-opening masonry infill wall, was developed by the RUAUMOKO [34] software. It is comprised of beam-column elements and a pair of nonlinear springs representing the lower infill panel, as illustrated in Fig. 12.

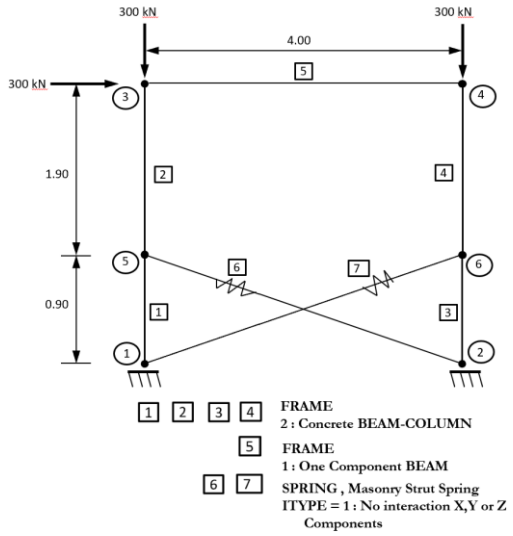

Fig. 12. Modelling of partial infilled RC frame with upper opening using RUAUMOKO.

To verify the proposed model of strengthened frames, the moment parameters shown in Tables 6 and 7 were used to model the partially infilled frames UPF-C and UPF-S for analyzing hysteresis behavior using the RUAUMOKO program [34], a non-linear structural analysis software, and the results were compared with the test data. The SINA degrading model was employed to simulate the beam and column members and to calculate their moment resistance. Additionally, the SINA model was used to analyze a partially infilled reinforced concrete (RC) frame with an upper opening.

The SINA degrading model represents a hysteretic behavior non-linear spring model, in which the structural members are simulated as equivalent compressive struts. In the non-linear analysis using RUAUMOKO, a cyclic lateral load was applied to replicate the forces experienced by the test specimen under laboratory conditions. Various parameters were incorporated into the software analysis, and the obtained values were compared with the results of the proposed model. The hysteresis behavior of the UPF-C and UPF-S specimens, as obtained from the analysis for verification, is shown in Figs. 13a, 13b, and 13c, respectively. These parameters are summarized in Table 8.

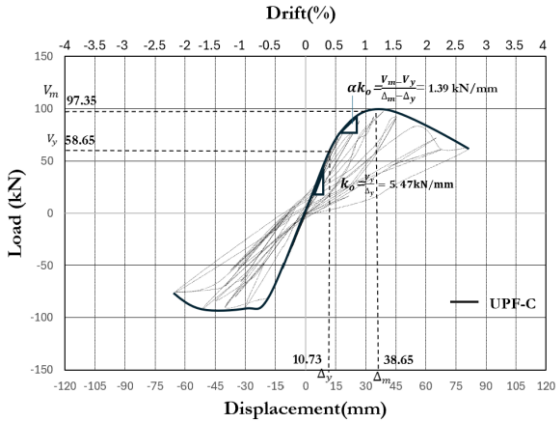

(a)UPF-C

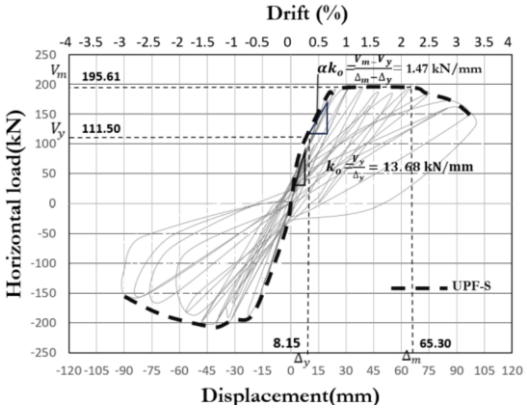

(a) UPF-S

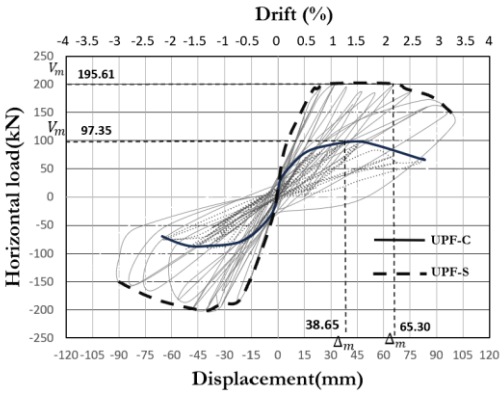

(e) UPF-C and UPF-S

Fig. 13. Enveloped curves analysis result of the RUAUMOKO program.

Table 8. Hysteresis behavior parameters in the UPF-C and UPF-S models from the enveloped curve analysis results.

Model	UPF-C	UPF-S
$k_o\,(kN/m)$	5.47	12.39
$V_y\,(kN)$	58.65	111.50
$\Delta_y\,(mm)$	10.73	8.15
$V_m\,(kN)$	97.35	195.61
$\Delta_m\,(mm)$	38.65	65.30
$\alpha k_o\,(kN/mm)$	1.39	1.51

Table 9 summarizes the hysteresis behavior parameters by comparing the laboratory test results with the analysis results obtained using the RUAUMOKO program for the UPF-C and UPF-S specimens. The analysis results from the model provided values very close to the maximum lateral resistance and initial stiffness observed in the laboratory tests, with differences of approximately 1.45% and 15.25%, respectively.

This indicates that the proposed model for the improved masonry wall structure can be effectively used

to evaluate the lateral resistance and stiffness of masonry wall structures with similar characteristics.

Table 9. Comparison of the UPF-C and UPF-S parameters from test results and analysis results.

Model	Experiment results		Analysis	
	UPF-C	UPF-S	UPF-C	UPF-S
$k_0\,(kN/m)$	5.92	14.28	5.47	12.39
$V_y\,(kN)$	67.05	112.65	58.65	110.25
$\Delta_y\,(mm)$	11.33	7.89	10.30	8.90
$V_m\,(kN)$	97.80	198.45	97.35	195.61
$\Delta_m\,(mm)$	45.13	67.30	38.65	65.30
$\alpha k_0\,(kN/mm)$	1.00	1.44	1.39	1.51

The hysteresis loops of both specimens are compared with the test results. Both sets of specimens are shown in Fig.s 14a and 14b. It was found that both sets of specimens align well with the laboratory test results, indicating that the proposed partial infilled frame with upper opening model can effectively be used to predict the resistance strength and stiffness values of the structures.

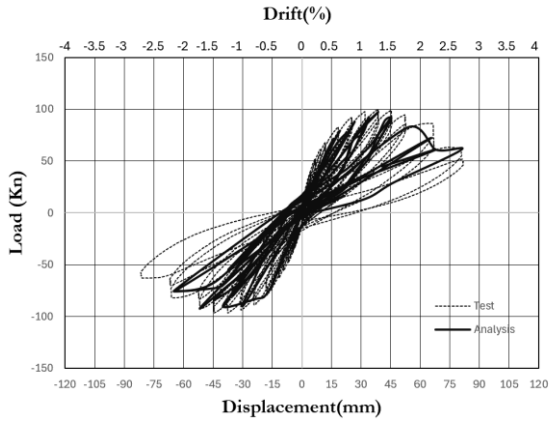

(a) UPF-C

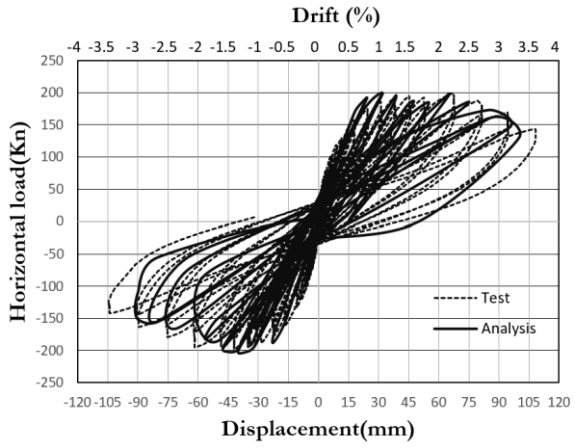

(b) UPF-S

Fig. 14. Hysteresis loops the Test result and Analysis of UPF-C and UPF-S.

To investigate the influence of individual retrofit components, additional numerical analyses were performed on two intermediate cases: (1) only infill panel strengthening without strengthening the RC frame (BF+WS), and (2) only frame strengthening without strengthening the masonry infill panel (BFS+W). The analysis results are outlined below.

1) BF+WS specimen.

The lateral resistance of the BF+WS model, which represents masonry infill panel strengthening without RC frame retrofitting, was evaluated through numerical simulation by replacing the strut forces of the original control wall spring (Component 6 in Fig. 12) with those of the strengthened wall spring. The resulting shear forces were plotted against lateral displacement to generate the hysteresis curve shown in Fig. 15a.

The specimen exhibited a maximum lateral resistance of approximately 106.93 kN and an initial stiffness of 6.33 kN/m, which increased approximately 9.84% and 15.72%, respectively, compared to the control specimen UPF-C. The results are summarized in Table 10.

2) BFS+W specimen.

The lateral resistance of the only frame strengthening scheme (BFS+W), without retrofitting the masonry infill panel, was numerically evaluated through simulation by replacing the lateral resistance of the control frame with that of the strengthened frame. The resulting shear forces were plotted against lateral displacement to generate the hysteresis curve for the BFS+W specimen, as shown in Fig. 13b.

The specimen exhibited a maximum lateral resistance and initial stiffness of about 186.03 kN and 6.55 kN/m, respectively, which increased 91.0% and 19.74% compared to the control specimen UPF-C. The results are summarized in Table 10.

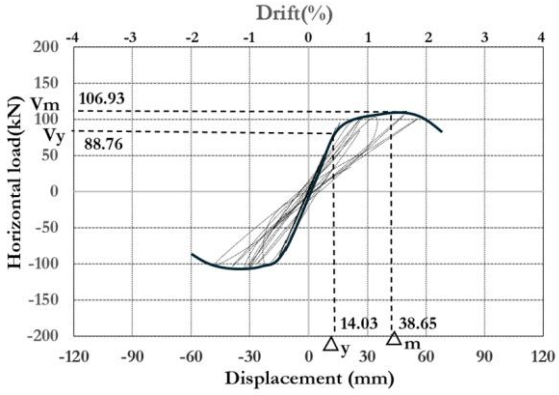

(a) BF+WS

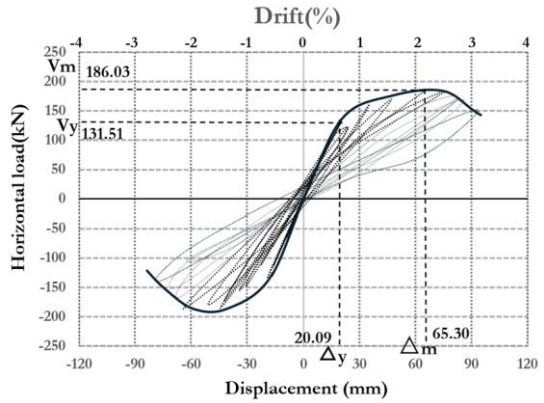

(b) BFS+W

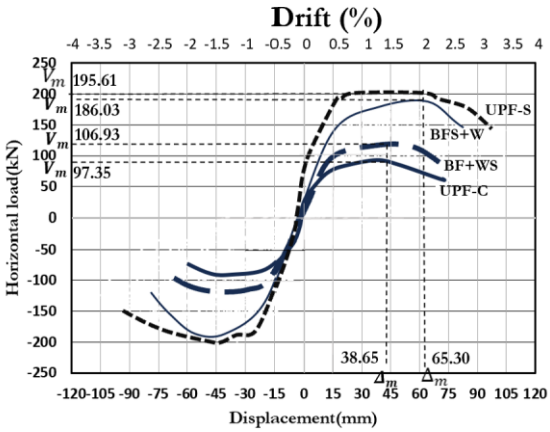

(c) UPF-C, BF+WS, BFS+W and UPF-S

Fig. 15. Enveloped curves analysis result of the RUAUMOKO program.

Table 10 presents a comparison of hysteresis loop parameters based on numerical analysis using RUAUMOKO software for the retrofitted specimens. The lateral resistance of the strengthened specimens: a) only strengthened infill panel (BF+WS), b) only strengthened frame (BFS+W), c) fully strengthened infilled frame (UPF-S), could be enhanced by 9.84%, 91.0%, 101%, respectively, compared to the control infilled frame (UPF-C).

The results indicate that the UPF-S specimen exhibits superior in the lateral resistance and stiffness when employed fully retrofitted frame and masonry infill panel, as illustrated in Fig. 15(c). This method provided an effective seismic strengthening strategy for masonry-infilled RC frames in high seismic zone.

Table 10. Comparison of the UPF-C, BF+WS, BFS+W and UPF-S parameters from analysis results of the RUAUMOKO program.

Model	UPF-C	BF+WS	BFS+W	UPF-S
$k_0\,(kN/m)$	5.47	6.33	6.55	12.39
$V_y\,(kN)$	58.65	88.76	131.51	111.50
$\Delta_y\,(mm)$	10.73	14.03	20.09	8.15
$V_m\,(kN)$	97.35	106.93	186.03	195.61
$\Delta_m\,(mm)$	38.65	38.65	65.30	65.30

4.5. Cost-Effectiveness and Implementation Considerations

The seismic retrofit scheme for each method depends on the seismic demand for each seismic hazard zone which can be determined according to the seismic code [35]. The resulting base shear demand serves as the target for evaluating the adequacy of retrofit strategies. In addition, the behavior of frame-wall interaction under earthquake load is also taken into consideration.

Based on the enveloped curve analysis results shown in Fig. 15, the control specimen (UPF-C) exhibited the lateral load capacity of 97.35 kN. The strengthened specimens BF+WS, BFS+W, and UPF-S enhanced the capacities to 106.09 kN, 186.03 kN, and 195.61 kN, respectively. Therefore, three alternative strengthening approaches can be suggested as follows:

1) BF+WS specimen: The only strengthened infill panel method increased the lateral resistance by 9.84%, compared to the control specimen (UPF-C). This method also improved the debonding between the column-wall interface, therefore it enhanced the ability to absorb the energy under cyclic loading. However, the column above the masonry level may be damaged by diagonal shear due to the short column effect under intense earthquake loading. This approach is suitable for low seismic hazard region with an economic cost (Table 11).

2) BFS+W specimen: This approach involves strengthening only the reinforced concrete frame without retrofitting the masonry infill panel. It increased the lateral resistance by 91% compared to the control specimen (UPF-C). However, the lack of strengthened masonry panel leads to infill failure characterized by diagonal compression cracks and separation at the wall-column interface resulting in substantial loss of lateral capacity. This method is recommended for regions with moderate seismic hazard with a medium cost (Table 11).

3) UPF-S specimen: This method involves strengthening both the structural frame (beams and columns) and the masonry infill panel. The retrofitted scheme demonstrates the highest performance, with 101% increase in lateral capacity compared to the control specimen (UPF-C). The masonry infilled frame significantly enhances the structural performance by improving strength, stiffness, and energy dissipation. It is the most effective scheme recommended for the high seismic hazard region with a reasonable cost (Table 11).

Table. 11. Comparison of estimated material costs for BF+WS, BFS+W, and UPF-S specimens.

No	Type Materials	BF+WS	BFS+W	UPF-S
1	DB12mm	-	1,260	1,260
2	RB 9mm	-	605	605
3	FB50x50x3m	-	170	170
4	L40x40x3mm	300	2,400	2,700
5	Exp. No.22	1,250	-	1,250
6	Exp. No.33	7,200	7,200	7,200
7	Cement	300	450	750
8	Sand	600	600	1,200
Total cost (THB)		9,650	12,685	15,135

It should be remarked that the experimental results from the control specimen with a partial infill wall (UPF-C) clearly demonstrated that the masonry infill is susceptible to diagonal compression failure and debonding at the column-wall interfaces, leading to premature separation from the frame. These findings indicated that the only frame retrofitted scheme is insufficient. The strengthened masonry infill panel with expanded metal mesh could enhance the tensile strength, stiffness, and energy dissipation capacity. While the strengthened column could reduce the diagonal shear damage in the column above the masonry level. Therefore, comprehensive retrofitting of both the frame and the infill wall is essential for effective seismic performance.

5. Conclusions

This experimental study aimed to investigate the behavior of masonry walls with upper openings in a reinforced concrete frame and to enhance their seismic resistance using ferrocement with expanded metal mesh. The key findings from the tests are summarized as follows:

a) The strengthened frame with ferrocement using expanded metal mesh and external steel reinforcement (UPF-S) significantly improved its yield strength and ductility. Compared to the unreinforced control specimen (UPF-C), UPF-S exhibited 1.68 times increase in yield strength and 1.94 times improvement in ductility, indicating a substantial enhancement in the frame's ability to resist deformation. Furthermore, the increased strength due to reinforcement resulted in the maximum resistance of UPF-S increased to 2.04 times higher than that of the existing partially infilled frame.

b) The strengthened frame UPF-S significantly improved its initial lateral stiffness (ko). This is reflected in the initial resistance to lateral loads compared to the unreinforced control specimen (UPF-C). The secant stiffness also increased which led to an enhancement in displacement capacity and ductility, allowing the structure to withstand greater deformations before failure.

c) The experimental results obtained for reinforced concrete frames with partial infill and an upper opening (UPF-C and UPF-S) validated the accuracy of the analytical model. The model's predictions closely matched the actual test results in terms of force and lateral displacement distributions, demonstrating its reliability. This suggests that the proposed model can be effectively applied for the design and evaluation of existing building frames with masonry openings, providing a predictive assessment of their resistance.

d) The test results confirmed the effectiveness of ferrocement with expanded metal mesh and external bar reinforcement in enhancing the bending resistance and ductility of infilled frame structures. The ferrocement layer delayed the onset of cracking and mitigated brittle shear failure, allowing the structure to absorb significant energy before failure. Additionally, it reduced the susceptibility of short columns to shear stress and altered their failure mode from brittle to ductile behavior.

Acknowledgement

This research was supported by the National Research Council of Thailand (NRCT), Sripatum University, and Chulalongkorn University Research Funds.

References

[1] A. S. M. Akid, M. H. Rashid, and M. H. R. Sobuz, "Effect of masonry infill wall with opening on reinforced concrete frame due to seismic loading: Parametric study," *International Journal of Structural Engineering,* vol. 11, no. 1,pp 84–105, 2020.

[2] S. Shan, S. Li, M. M. Kose, H. Sezen, and S. Wang, "Effect of partial infill walls on collapse behavior of reinforced concrete frames," *Engineering Structures,* vol. 197, p. 109377, 2019.

[3] S. Calderón, C. Sandoval, E. Inzunza, C. Cruz-Noguez, A. B. Rahim, and L. Vargas, "In fluence of a window type opening on the shear response of partially grouted masonry shear walls," *Engineering Structures,* vol. 201, p. 109783, 2019.

[4] S. H. Basha, S. Surendran, and H. B. Kaushik, "Empirical models for lateral stiffness and strength of masonry-infilled RC frames considering the influence of openings," *Journal of Structural Engineering*, vol. 146, no. 4, p. 04020021, 2020.

[5] A. Messaoudi, R. Chebili, H. Mohamed, and H. Rodrigues, "Influence of masonry infill wall position and openings in the seismic response of reinforced concrete frames," *Applied Sciences*, vol. 12, no. 19, p. 9477, 2022.

[6] A. Leeanansaksiri, P. Panyakapo, and A. Ruangrassme, "Seismic capacity of masonry infilled RC frame strengthening with expanded metal ferrocement," *Engineering Structures*, vol. 159, pp. 110-127, 2018.

[7] S. Longthong, P. Panyakapo, and A. Ruangrassamee, "Seismic strengthening of RC frame and brick infill panel using ferrocement and expanded metal," *Engineering Journal*, vol. 24, no. 3, pp. 45–59, 2018.

[8] S. V. S. Jebadurai, D. Tensing, and C. F. Christy, "Enhancing performance of infill masonry with skin reinforcement subjected to cyclic load," *International Journal of Engineering*, vol. 32, no. 2, pp. 224–230, 2019.

[9] T. Choudhury and H. B. Kaushik, "Experimental evaluation of full-scale URM buildings strengthened using surface-mounted steel bands," *Journal of Structural Engineering,* vol. 147, no. 2, 2021.

[10] S. H. Ahmed and M. R. Abdulkadir, "In plane shear strengthening of clay masonry walls with opening," *Sulaimani Journal for Engineering Sciences,* vol. 7, no. 1, pp. 49–64, 2020.

[11] X. Yao, Z. X. Guo, S. H. Basha, and Q. Huang, "Innovative seismic strengthening of historic masonry walls using polymer mortar and steel strips," *Engineering Structures,* vol. 228, p. 111507 , 2021.

[12] T. El Salakawy and G. Hamdy, "Experimental and numerical investigation of strengthening of openings in masonry walls using steel bars and steel wire mesh," *European Journal of Environmental and Civil Engineering,* vol. 26, no. 15, pp. 7461–7479, 2022.

[13] L. Perez-Pinedo, C. Sandoval, R. Alvarado, L. Vargas, S. Calderon, and E. Bernat, "Seismic strengthening of partially grouted masonry walls with openings: Evaluation of ferrocement and BTRM solutions," *Journal of Building Engineering,* vol. 88, p. 109235, 2024.

[14] S. B. Kadam, Y. Singh, and B. Li, "Experimental investigations on masonry buildings strengthened using ferro-cement overlay under dynamic loading," *ISET Journal of Earthquake Technology,* vol. 57, no. 1, pp. 1–16, 2020.

[15] W. Warlarpih, "Shear behavior of Autoclaved Aerated Concrete (AAC) masonry walls with and without openings strengthened with welded wire mesh," *Structural Engineering and Mechanics,* vol. 87, no. 5, pp. 487–498, 2023.

[16] F. A. Ismail, A. Hakam, and A. Alfajri, "Study on the behavior of a simple house partially retrofitted using ferrocement layers due to earthquake loads," *International Journal on Advanced Science, Engineering & Information Technology,* vol. 13, pp. 501, 2023.

[17] A. Hasnat, R. Ahsan, and S. M. Yashin, "Quasi static in-plane behavior of full-scale unreinforced masonry walls retrofitted using ferrocement overlay," *Asian Journal of Civil Engineering,* vol. 23, pp. 649–664, 2022.

[18] S. Ivorra, B. Torres, F. J. Baeza, and D. Bru, "In plane shear cyclic behavior of windowed masonry walls reinforced with textile reinforced mortars," *Engineering Structures,* vol. 226, p. 111343, 2021.

[19] T. Li, M. Deng, Y. Ma, and Y. Zhang, "In-plane behavior of URM wall with openings strengthened with ECC subjected to cyclic load," *Structures*, vol. 34, pp. 2765–2776, 2021.

[20] F. A. Ismail, A. Hakam, J. V. Osman, and D. Syandriaji, "Experimental study on the retrofitting of damaged hollow brick masonry houses using a ferrocement layer," *International Journal of Geomate,* vol. 25, no. 111, pp. 254–261, 2023.

[21] S. Panyamul, P. Panyakapo, and A. Ruangrassamee, "Seismic shear strengthening of reinforced concrete short columns using ferrocement with expanded metal," *Engineering Journal,* vol. 23, no. 6, pp. 175–189, 2019.

[22] K. Murugan and A. K. Sengupta, "Seismic performance of strengthened reinforced concrete columns," *Structures,* vol. 27, pp. 487–505, 2020.

[23] A.-E.-R. M. Ahmed, O. A. Farghal, M. M. Ahmed, and A. M. Hamed, "Structural behavior of normal RC rectangular short columns strengthened using ferrocement system," *IJEDR - International Journal of Engineering Development and Research,* vol. 9, no. 1, pp. 247–256, 2021.

[24] P. S. Theint, A. Ruangrassamee, and Q. Hussain, "Strengthening of shear-critical RC columns by high strength steel-rod collars," *Engineering Journal,* vol. 24, no. 3, pp. 107–128, 2020.

[25] *Guide for the Design, Construction, and Repair of Ferrocement*, ACI 549.1R-93, ACI Committee, American Concrete Institute, MI, USA.

[26] G. Tumialan, K. Nakano, H. Fukuyama, and A. Nanni, "Japanese and North American guidelines for strengthening concrete structures with FRP: A comparative review of shear provisions," in *FRPRCS-5: Fibre-Reinforced Plastics for Reinforced Concrete Structures, Proc. 5th Int. Conf. Fibre-Reinforced Plastics for Reinforced Concrete Structures, Cambridge*, U.K., Jul. 16–18, 2001, vol. 1, pp. 457–466.

[27] A. Saneinejad and B. Hobbs, "Inelastic design of infilled frames," *J Struct Eng ASCE*, vol. 6682, pp. 634 –50, 1995.

[28] *Standard Test Method for Compressive Strength of Hydraulic-Cement Mortars*, ASTM Standard No. ASTM C349, American Society for Testing and Materials (ASTM), 1997.

[29] *Steel Bars for Reinforced Concrete: Deform Bars*, TIS 24-2559, Thai Industrial Standard (TIS), Department of Industrial Product Standard, Ministry of Industry, Thailand, 2016.

[30] *Steel Bars for Reinforced Concrete: Round Bars*, TIS 20-2543, Thai Industrial Standard (TIS), Department of Industrial Product Standard, Ministry of Industry, Thailand, 2000.

[31] *Expanded Metal Standard by Japanese Industrial Standard*, JIS Standard No. JIS G3351, Japanese Standards Association, 1987.

[32] Federal Emergency Management Agency, "Interim testing protocol for determining the seismic performance characteristics of structural and nonstructural components," Redwood City, Report no. FEMA 461, 2007.

[33] *Seismic Rehabilitation of Existing Building*, ASCE Standard No. ASCE/SEI 41–06, American Society of Civil Engineers (ASCE), 2006.

[34] A. J. Carr. *RUAUMOKO Computer Program.* University of Canterbury, Christchurch, New Zealand, 2006.

[35] *Standard for Seismic Design of Buildings,* DPT 1301/1302-61, Bangkok, Ministry of Interior, Thailand, 2018.

Rattawit Amornpunyapat received B.Eng. in Civil Engineering from Kasembundit University, Bangkok, Thailand in 1997, and M.Eng. in Civil Engineering from Sripatum University, Bangkok, Thailand in 2000.

He has worked in the construction industry as a civil engineer since 1997. His experience involves the construction of buildings and infrastructures. Since 2015, he has been a student in Docter of Engineering Program in Civil Engineering, Sripatum University. His research interests include seismic strengthenening of buildings.

Phaiboon Panyakapo hold Doctor of Engineering from AIT since 1999. He has been graciously recieved Professor of Civil Engineering since 2018. He is a committe in the Engineering Institute of Thailand. He also involved in the improvement of earthquake resistant design standard of Thailand. His research involed in the seismic analysis and design, seismic strengthening of building.

Anat Ruangrassamee received the B.Eng. degree in civil engineering from Chulalongkorn University, Bangkok, Thailand and the M.Eng. and Ph.D. degrees in civil engineering from Institute of Science Tokyo (Formerly, Tokyo Institute of Technology), Japan. Currently, he is a professor at Department of Civil Engineering, Chulalongkorn University. His research interests include earthquake engineering and seismic retrofit of structures.

Pochara Kruavit received the Ph.D. degree in Civil Engineering from Chulalongkorn University, Thailand, in 2019. He has worked at Department of Civil Engineering King Mongkut's University of Technology North Bangkok. His research interests include nonlinear analysis, seismic behaviour and strengthening of reinforced concrete structure.